

ARTICLE OPEN



Photo-oxidation of PE-HD affecting polymer/fuel interaction and bacterial attachment

Maren Erdmann¹, Sherin Kleinbub¹, Volker Wachtendorf¹ , Jan David Schutter¹, Ute Niebergall¹, Martin Böhning¹ and Andrea Koerdt¹

In the present study, a simple approach was used to investigate the effect of UV-exposure on two high density polyethylene materials (PE-HD), commonly used for storage tanks, on fuel sorption behavior and colonization by microorganisms. The aim was to investigate whether the sorption behavior of the fuels (diesel/biodiesel) and the colonization by microorganisms, frequently occurring in the fuel, is affected and may lead to undesirable or safety-relevant material changes. We showed that the UV-irradiation leads to significant changes of the sorption behavior due to chemi-crystallization and crosslinking. The fuel sorption is affected by the UV-induced formation of polar carbonyl and hydroxyl groups predominantly occurring at the surface. With respect to microbial colonization behavior for *Bacillus subtilis* and *Pseudomonas aeruginosa*, isolated from a contaminated diesel sample, differences of the initial adhesion could be shown depending on the initial type of polyethylene as well as on the degree of UV-induced degradation.

npj Materials Degradation (2020)4:18; <https://doi.org/10.1038/s41529-020-0122-1>

INTRODUCTION

Environmentally friendly energy sources, alternatives to conventional fuel, are becoming increasingly important. Consequently, an increase in improvement, production, and use of biodiesel (BD) has been observed in the last decades. However, less attention has been paid to the polymeric storage tanks, manufactured from semi-crystalline high-density polyethylene (PE-HD), which were originally designed for conventional fuel. PE-HD has become one of the most important polyolefins for storage tanks due to its low-cost production, variability in physical/mechanical properties and high chemical resistance, while the oxidative stability needs to be improved by stabilizers. Nowadays, those tanks are used for the storage of both, although BD and conventional diesel fuel show differences e.g. in the chemical composition, polarity, viscosity, energy density. It is conceivable that the tanks designed for diesel are not necessarily suitable for the storage of BD and that the storage of BD may lead to undesirable effects, which in extreme cases represent a safety risk.

The combined action of ultraviolet (UV) radiation and oxygen on PE-HD is widely understood and here termed as photo-oxidative degradation¹, which follows the auto-oxidation mechanism². Theoretically, polyolefins are transparent to UV radiation^{3,4}. Therefore, the existence of chromophores as radiation absorbing species is imperative for the incipient chemical reaction, e.g., additives, hydroperoxides, saturated, and unsaturated carbonyl groups^{4,5} previously formed by thermo-oxidation during processing. Common oxidation products resulting from the UV-induced photo-oxidation include hydroperoxide (-OOH), hydroxyl (-OH), carboxylic acid (-COOH) and ketone groups (C=O)^{4,6,7}, which can be monitored by several methods comprising spectroscopic techniques, e.g., FT-IR⁷⁻⁹, UV-vis or luminescence emission¹⁰.

Apart from molecular changes, the photo-oxidation can alter the macromolecular architecture of the hydrocarbon chain, leading to chain scission and/or crosslinking predominantly in the amorphous regions^{4,11,12}. The oxidation starts at the surface and reaches deeper layers with ongoing exposure, where the

reaction rate competes with the diffusion of oxygen into the material and diffusion limited oxidation (DLO) can occur. Especially the degradation of tie-molecules and entanglements interconnecting adjacent crystalline lamellae leads to a significant diminishing of mechanical properties. After the end of an induction period, the polymer can undergo an abrupt ductile-brittle transition, which is characterized, e.g., by a significant reduction in elongation at break^{9,11,13-15} or the loss of impact strength^{15,16}.

The PE-HD/fuel interactions on a previously UV-degraded polymer have not been in the focus so far. In addition to conventional petroleum diesel fuel, BD is increasingly used as renewable fuel. Both fuels can be absorbed by the amorphous regions of PE-HD¹⁷⁻²⁰. The fuel mass uptake depends on the fuel composition, especially on its polarity^{18,20}, the crystallinity of the polyethylene^{20,21} and the immersion temperature¹⁸. The fuel sorption in PE-HD causes a plasticizing effect¹⁸ that changes the tensile properties, e.g., yielding¹⁹⁻²² and leads to a fuel-induced transparency on the plastically deformed regions²³. With regards to long-time polymer/fuel-interactions in storage applications, a BD-induced acceleration of the oxidation of PE-HD ('co-oxidation') has been confirmed previously^{20,24,25}.

The microbiological contamination of fuel, called diesel-pest, occurs due to the ability of certain types of microorganisms to metabolize fuel and using it as carbon/energy-source for their growth²⁶⁻³¹. The water absorption capacity, especially of BD, provides the further basic requirement for microbiological activity^{32,33}. The best-known representatives of a diesel-pest are facultatively anaerobic members of the genera *Bacillus*, *Pseudomonas*, *Enterobacter*, and *Staphylococcus*^{28,34}. The degrading biological activity can lead to fuel degradation, termed biofouling, in the fuel lines and possibly in the fuel storage tanks themselves³⁴. Microbial contamination is not only a problem for the fuel itself but may also affect the quality of the fuel storage tanks.

¹Bundesanstalt für Materialforschung und -prüfung (BAM), Unter den Eichen 87, 12205 Berlin, Germany. ✉email: andrea.koerdt@bam.de

For *Bacillus* and *Pseudomonas*, it has been demonstrated that polyethylene can be used as carbon source^{31,35}. Especially, through photo-oxidation and thermal treatment pre-aged polypropylene and low-density polyethylene showed a susceptibility to microbial degradation^{35,36}. A similar situation could apply to pre-aged PE-HD. Usually, spatial proximity to the substrate, typically in the form of a biofilm, is a prerequisite for such a material damage. As biofilm formation begins with the initial attachment of the cells to the substrate it is reasonable to investigate this stage at first. The attachment process is divided into two steps:

(1) The first step is the reversible attachment, where cells bind to the substrate by weak forces such as van der Waals forces, electrostatic forces, or hydrophobic interactions.

(2) The second step is the irreversible attachment, where a repositioning of the cell and surface structures occurs. Furthermore, adhesin molecules are produced that may lead to the formation of covalent bonds between cell and substrate. The specific mechanisms are very complex and depend on the bacterial strain and the environmental conditions^{37–39}.

The following scenario is assumed in this study: Two different grades of PE-HD, commonly used for fuel tanks, are chosen which e.g. differ in their crystallinity and stabilizer content. Both PE-HD are temporarily stored outside and exposed to environmental influences. Due to the combined effect of the UV component of solar radiation and oxygen from the ambient air, the PE-HD undergoes auto-oxidation².

An important condition for biological activity is the presence of water, which is given in the described scenario: outside by rainfall and inside the polymer tank by the accumulation of condensed atmospheric moisture (in BD to a greater extent)^{32,33}. In- and outside of the tank microorganisms are naturally abundant and when conditions facilitate their growth they can be involved in the degradation of the polymer and the fuel^{26–31}. A prerequisite for this growth and the formation of a destructive biofilm is the initial attachment of the microorganisms to the substrate.

In a simplified approach, the following key issues are attempted to be addressed: (1) does the fuel sorption of the two different PE-HD types change when previously damaged by UV-irradiation; (2) does the possibly different absorption of diesel or BD lead to changes in the material resistance; (3) do microorganisms extracted/isolated from a diesel-pest adhere differently to the surface of the two polymer types; (4) does the UV-induced photo-oxidation of the polymers lead to a change of the adhesion of these microorganisms, which under real conditions finally leads to a destructive biofilm.

RESULTS AND DISCUSSION

Fuel sorption kinetics on photo-oxidized PE-HD

Several studies showed that semi-crystalline PE-HD can absorb fuel, e.g. petroleum diesel^{18–20,23} and BD^{17–20}. Changes of the fuel sorption kinetics of PE-HD due to photo-oxidation have not been in the focus so far. With respect to our simulated fuel storage scenario, we selected two unpigmented opaque PE-HD materials applicable for container tanks^{16,20}. The polymers were exposed to UV radiation. The highest applied UV-irradiation energy, i.e., the UV-radiative exposure H of 460 MJ m^{-2} corresponds to ~ 2 years of outdoor exposure in the south of Florida (solar radiation of 280 MJ m^{-2} /year (see Methods) not considering the higher temperature in the artificial weathering device of 60°C). Typical wall thicknesses for such container tanks made from PE-HD are usually in the range of $1.5\text{--}2.5 \text{ mm}$ ⁴⁰, even for large intermediate bulk containers. Pre-aged disks with UV radiation (thickness of 1 mm) were chosen as a suitable geometry (plane sheet) for the fuel sorption experiments. The sorption temperature of 60°C corresponds to the upper temperature limit recommended for testing the fuel permeability into polymers (industry standard SAE J2665⁴¹).

General quantities to evaluate the polymer/fuel interaction are the fuel equilibrium concentration c_∞ and the diffusion coefficient D . The fuel sorption curves of non-exposed PE-HD1 and PE-HD2 follow the Fick's law, i.e., the fuel mass uptake is fast at the beginning and slows down until an equilibrium concentration is reached after $\sim 150 \text{ h}$ (Fig. 1a).

The values estimated for the two polymers (based on fitting of Eq. 3 for plane-sheet geometry to the experimental data points) are summarized in Table 1. The applicability of Fickian sorption according to Eq. 3 is proven by plotting the concentration vs. the square root of time (Supplementary Fig. 1). The observed linear behavior of the initial part of the curve indicates Fickian behavior in contrast to a distinct S-shape expected for inhomogeneous media or strongly concentration-dependent diffusivity. Using desorption for assessing the diffusivity is not favorable, at least for BD, due to the limiting evaporation of the desorbed fuel from the surface¹⁸.

The sorption curves in Fig. 1a clearly reflect the effect of the differences in fuel composition, expressed in an almost twofold higher equilibrium concentration $c_{\infty,D}$ of the non-polar diesel compared to more polar BD $c_{\infty,BD}$ ^{18–20} (rapeseed methyl ester). The diesel diffusion coefficient D_D into both non-exposed polymers is also almost twice as fast as for BD D_{BD} (Table 1).

The difference in crystallinity X_c between the two non-exposed polymers (Table 2) is also evident in the mass uptake curves (Fig. 1a). Higher fuel equilibrium concentrations and faster fuel diffusion rates were determined for PE-HD1, which has a lower

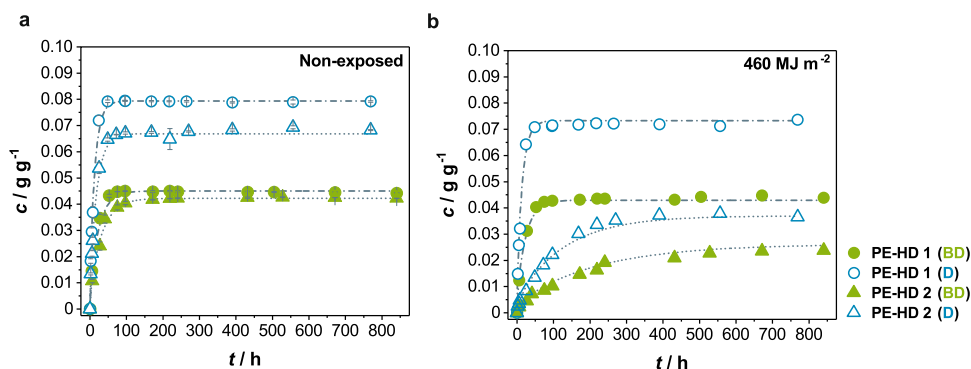


Fig. 1 Fuel concentration in PE-HD1 and PE-HD2 immersed in biodiesel (BD) and diesel (D). Mass uptake for **a** a non-exposed sample and **b** after an UV-radiation exposure of 460 MJ m^{-2} . The immersion temperature was $T = 60^\circ\text{C}$ using a plane sheet geometry ($h = 1 \text{ mm}$). Error bars represent standard deviation of sample replicates. For non-exposed ($H = 0 \text{ MJ m}^{-2}$) samples, $n = 3$ replicates for PE-HD1 and $n = 2$ replicates for PE-HD2, for $H = 460 \text{ MJ m}^{-2}$ exposed samples one replicate each for both PE's. Lines always represent the fit of Eq. 3 to the data points.

Table 1. Determined equilibrium concentrations C_∞ in g g^{-1} and estimated diffusion coefficients D in $\text{cm}^2 \text{s}^{-1}$ for non-exposed ($H = 0 \text{ MJ m}^{-2}$) and for UV-radiative exposure $H = 460 \text{ MJ m}^{-2}$ for PE-HD1 and PE-HD2 in biodiesel (BD) and diesel (D) for plane sheet geometry ($h = 1 \text{ mm}$).

		PE-HD1		PE-HD2	
		Non-exposed	460 MJ m^{-2}	Non-exposed	460 MJ m^{-2}
BD	c_∞	0.0443	0.0439	0.0424	0.0255
	D	$2.25 \cdot 10^{-8}$	$1.64 \cdot 10^{-8}$	$1.52 \cdot 10^{-8}$	$0.12 \cdot 10^{-8}$
D	c_∞	0.0792	0.0737	0.068	0.0365
	D	$3.30 \cdot 10^{-8}$	$2.29 \cdot 10^{-8}$	$2.25 \cdot 10^{-8}$	$0.26 \cdot 10^{-8}$

Table 2. Compilation of properties for both investigated PE-HD.

		PE-HD1	PE-HD2
Melt flow rate ^a (190 °C, 21.6 kg)	/g (10 min) ⁻¹	6	23
Melting peak temperature ^b T_m^{DSC}	/°C	134	139
Crystallinity ^b χ_c^{DSC}	/%	72	79
OIT ^b at 180 °C	/min	436	74
Notched Charpy impact strength ^c a_{cN} at -30 °C instrumented determined	/kJ m ⁻²	16	19
Yield stress ^b σ_y	/MPa	25	32
Yield strain ^b ϵ_y	/%	11	9

^aFrom technical data sheet.

^bFrom ref. 20.

^cFrom ref. 16.

degree of crystallinity, i.e., a larger amorphous volume fraction that can absorb the fuel, compared to PE-HD2. Such crystallinity dependence of the fuel equilibrium concentration is consistent with other studies^{20,21}. Hence, there is an inverse relationship between crystallinity, fuel saturation concentration, and diffusivity.

The combination of UV radiation and oxygen on PE-HD can lead to photo-oxidative degradation inducing molecular changes and alter the macromolecular architecture of the hydrocarbon chains^{4,11,12}. The photo-oxidation starts at the surface and upon widening into deeper layers of the material competes with the transport of oxygen into the solid resulting in DLO.

The fuel sorption curves of both photo-oxidized polyethylenes exposed to a UV-radiative exposure $H = 460 \text{ MJ m}^{-2}$ are depicted in Fig. 1b. The course of the BD uptake for photo-oxidized and non-exposed PE-HD1 are almost identical; the maximum diesel concentration c_∞ is only slightly lower for the UV-exposed PE-HD1. As shown in Erdmann et al., PE-HD1 predominately undergoes chain-scission when exposed to UV-irradiation but to a minor extent since the polymer presents a good resistance to photo-oxidation (verified by a high OIT)¹⁶. The photo-oxidative degradation on PE-HD1, preferentially near the surface (DLO), does not affect the BD concentration, while the diesel concentration decreases with progressive UV-exposure (Fig. 2a/Table 1). Both diffusion coefficients show a continuous decrease with UV-exposure (Fig. 2b). The observed outlier at 330 MJ m^{-2} in BD may be due to heterogeneity of degradation and/or to possible measurement errors caused by the lower uptake in PE-HD1.

In contrast, the fuel mass uptake in Fig. 1b of the photo-oxidized PE-HD2 is significantly slower compared to the non-exposed polymer. Both fuel equilibrium concentrations c_∞ are almost reduced to 50% of the initial value and reached within a distinctly longer immersion time (Fig. 1b/Table 1). The diffusion rates are drastically decelerated to about one tenth. PE-HD2

possesses a distinctly shorter OIT that rapidly diminishes upon UV-irradiation¹⁶, indicating a significantly lower stabilization against oxidation. Following UV-induced chain-scission, PE-HD2 predominately undergoes significant chemi-crystallization¹⁶. The formed short chain fragments have an enhanced mobility enabling further crystallization⁴. Consequently, the content of amorphous fraction is reduced. The drastically reduced fuel concentration and the slower diffusivity already after the lowest UV-exposure of 110 MJ m^{-2} in the case of PE-HD2 (Figs 1 and 2) is because fewer fuel diffuses into the amorphous regions. Both characteristic sorption values remain constant on their respective low plateau upon further UV-exposure. To summarize, the changes of the sorption parameters in Figs 1 and 2 for both photo-oxidized polymers can be directly related to changes in their molecular, macromolecular, and morphological structure resulting from the UV-induced degradation.

Characterization of the UV-induced degradation

It is generally agreed that the initiating step for oxidation is the formation of a polymer alkyl radical (P^*) by abstraction of a hydrogen atom. In the presence of air, this alkyl radical (P^*) further reacts with oxygen (O_2) to a polymer peroxy radical (POO^*), polymer hydroperoxide (POOH) and/or hydroxy radical (HO^*)⁴. These photo-oxidation products cause the initial non-polar polyethylene to become increasingly polar. The UV radiation reaches the surface of the UV-facing side of the specimen with the highest irradiance and is absorbed increasingly by polyethylene, chromophores, and stabilizers upon entering deeper layers and only a fraction reaches the backside (see absorption spectrum Supplementary Fig. 2).

Molecular changes of PE-HD induced by photo-oxidation can be monitored by the build-up of carbonyl and hydroxyl groups as revealed by the evolution of characteristic absorption bands in FT-IR/ATR (Supplementary Fig. 3). The identified carbonyl absorption bands include those characteristics for ester, aldehyde, carboxylic acid, and ketone groups¹⁶. The integration of this spectral region defined as carbonyl index CI is frequently used as a measure of the extent of degradation, although the ATR technique only covers a thin surface layer it may be considered representative for the overall progression of the degradation. The presented hydroxyl index HI may also include hydroperoxides, which appear in the same wavenumber range.

The indices (HI , CI) for each polyethylene evolve similar during UV-irradiation (Fig. 3a). PE-HD1 presents a gradually increasing CI and HI and a long induction period. Contrary, both indices for PE-HD2 show a rapid non-linear increase. For the longest exposure (500 MJ m^{-2}), the CI value of PE-HD2 is by more than a factor of three higher compared to PE-HD1. This is accompanied by a slower and reduced fuel sorption indicated by changes of c_∞ and D due to the formation of polar oxygen containing groups reducing the interaction with the non-polar diesel, chemi-crystallization and partial crosslinking. Thus, the photo-oxidized regions of polyethylene, expected preferably at the surface layer, are assumed to have a lower fuel solubility than the non-oxidized regions in the interior of the polyethylene sample. Nevertheless, this induced layered inhomogeneity does not manifest itself in the sorption kinetics. Although the equilibrium concentration and the diffusivity are distinctly affected, the mass uptake follows still Fickian behavior, i.e., the initial course of the uptake vs. square root of time is linear (see Supplementary Fig. 1) and the data points can be fitted well by Eq. 3 allowing the estimation of diffusion coefficients.

The abrupt decrease of both sorption quantities, D and c_∞ , for PE-HD2 goes along with the sudden increase of the bulk density ρ^* already for the lowest UV-radiative exposure H of 110 MJ m^{-2} (Fig. 3b), while PE-HD1 presents a gradually density raise with H . This density increase can also be caused by the incorporation of

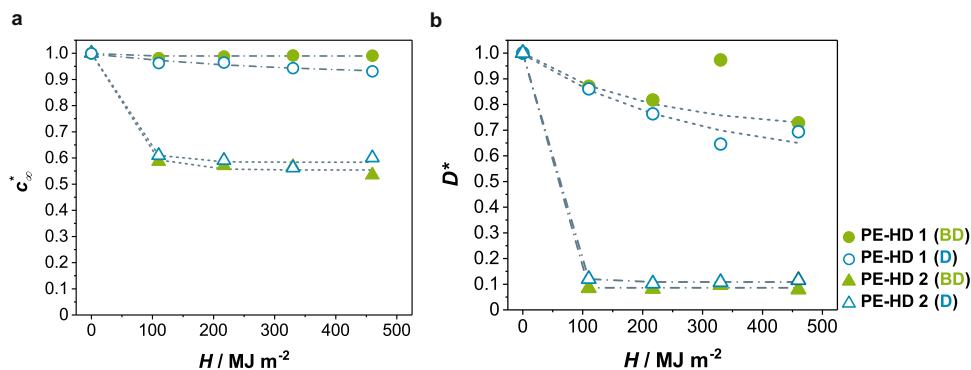


Fig. 2 Progression of sorption parameters for increasing UV-radiative exposure. In **a** the normalized equilibrium concentrations and in **b** the normalized diffusion coefficients for UV-radiative exposures up to 460 MJ m^{-2} of PE-HD1 and PE-HD2 are shown. The immersion temperature was $T = 60^\circ\text{C}$ using a plane sheet geometry ($h = 1 \text{ mm}$). Sorption parameters are normalized to their initial values (indicated by an asterisk) to highlight the differences.

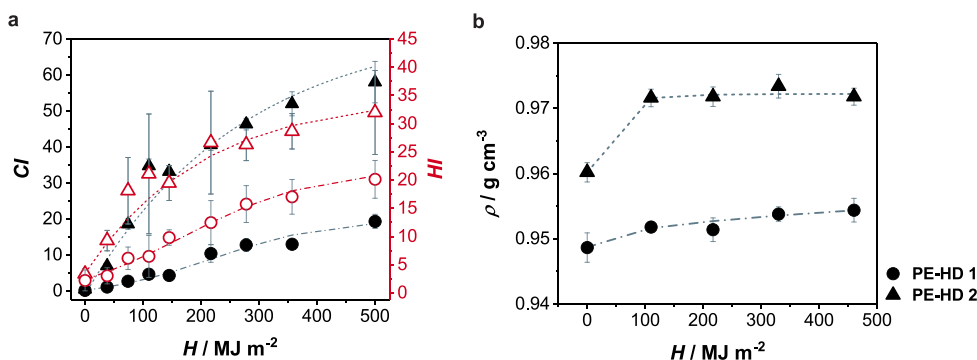


Fig. 3 Progression of degradation for increasing UV-radiative exposure. The results of **a** carbonyl index CI and hydroxyl index HI , and **b** density ρ for UV-radiative exposure up to 500 MJ m^{-2} for PE-HD1 and PE-HD2 are demonstrated. The carbonyl index and hydroxyl index were determined on the UV lamp-facing side of the samples. The figure was drawn after data from ref. ¹⁶. Standard error of the mean value of $n = 6$ replicates (CI , HI) and of $n = 4$ replicates (ρ).

the heavier oxygen into the polymer matrix resulting from the abstracted hydrogen by the photo-oxidation^{42,43} and by chemi-crystallization since crystals are more densely packed than amorphous regions^{43,44}.

The density increase through chemi-crystallization is a direct result of chain scission caused by UV-irradiation and occurs predominantly at the surface. In contrast, the obtained values represent the overall density of the samples, which nevertheless reflect significantly changes in the fuel sorption with increasing exposure H (cf. Figs 1b and 2).

The UV-induced degradation on the surfaces of both polyethylenes is also accompanied by an increase of surface roughness, leading partly to larger scattering of the FTIR-based CI and HI (Fig. 3a). A common approach to determine the surface roughness Rq (root mean square, RMS) is the evaluation of AFM-derived topography profiles. The roughness was determined in an area of $50 \times 50 \mu\text{m}^2$ (Supplementary Figs. 4 and 5). Both non-exposed PE-HD surfaces already have an initial roughness Rq of about 50 nm, due to the manufacturing process. The surface roughness increases by more than a factor of two with UV-exposure. This effect is again more pronounced on PE-HD2 than on PE-HD1.

Initial attachment of bacterial strains on photo-oxidized PE-HD surfaces

In the course of finding environmentally friendly ways to deal with the large amounts of polymer waste, microorganisms have been identified that can actively degrade polymers and use the long hydrocarbon-chain as carbon source. Polymers that have been pre-aged by UV radiation appear to be more susceptible to

microbiological degradation. Both polypropylene and low-density polyethylene were better degraded after pre-ageing with UV radiation by *Pseudomonas* and *Bacillus* species respectively than untreated Polymers^{35,36}. Interestingly, for both species type strains are known that can use the hydrocarbon chains of fuel as sole carbon source as well²⁸.

In the present study, we have investigated whether *Bacillus subtilis* and *Pseudomonas aeruginosa*, isolated from a diesel pest and known to degrade fuel, prefer the attachment on photo-oxidized compared to non-oxidized PE-HD surfaces. Initial attachment is a process that takes place within seconds to a few minutes, with the transition from reversible to irreversible being dynamic and difficult to determine over time. Therefore, the cells and the material were incubated for 10 min, unless indicated otherwise.

The semi-crystalline character and the specimen thickness, here $h \geq 4 \text{ mm}$, showed PE-HD as an opaque/non-transparent material under visible radiation^{20,23}. Thus, optical light transmission microscopy is not an appropriate method to count adherent bacteria. In our first approach to evaluate the initial attachment on the two photo-oxidized PE-HDs, the adherent bacteria (DNA/RNA) were stained with a fluorescent agent, DAPI (4',6-Diamidino-2-Phenylindole) with an emission wavelength of $\lambda_{em} = 461 \text{ nm}$, that can be visualized and counted under a fluorescence microscope.

Exemplary images in Fig. 4a, b shows that *B. subtilis* adheres on both polymers (non-exposed and exposed with $H = 500 \text{ MJ m}^{-2}$). Noticeably, not only the rod-shaped *B. subtilis* fluoresces, but also small bright heterogeneous areas appear on both photo-oxidized

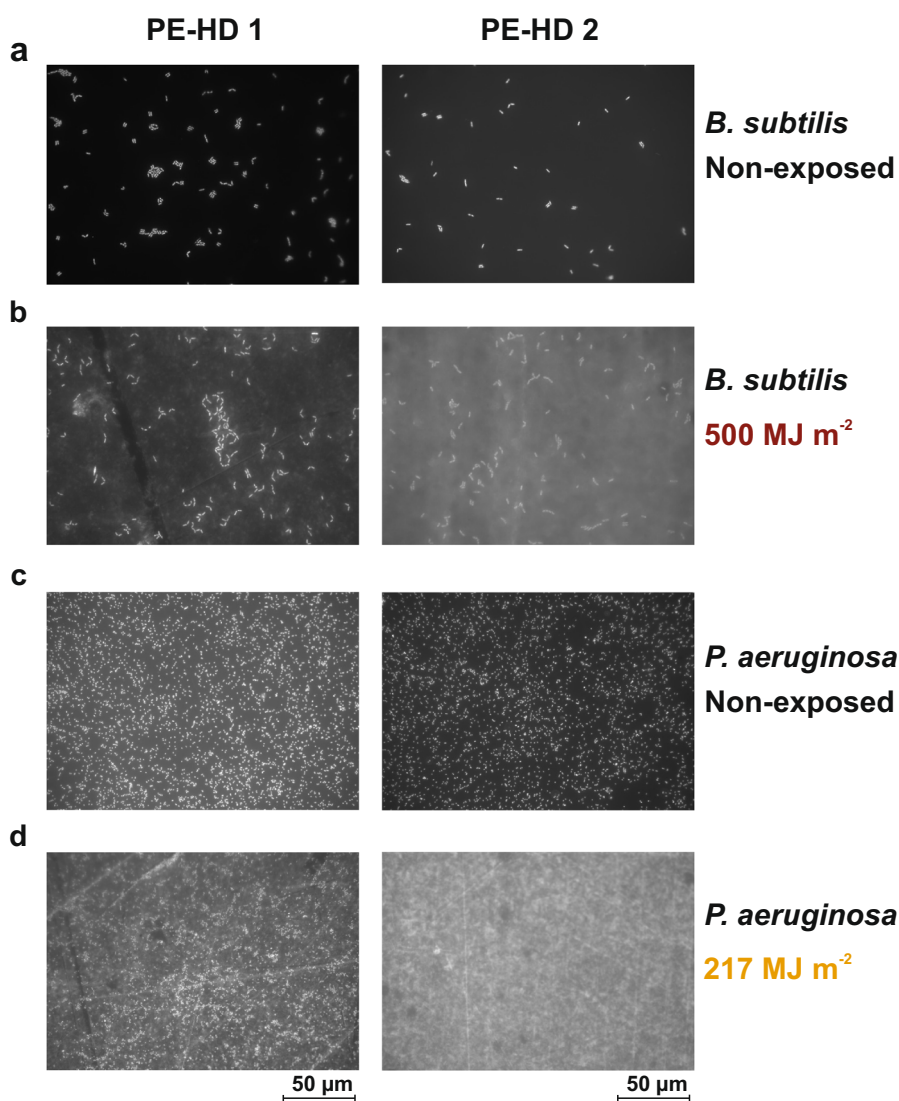


Fig. 4 Fluorescence microscopic view of the different colonization by microorganisms on UV-exposed polymer surfaces. Initial adhesion of *B. subtilis* after attachment time of 10 min on PE-HD1 (left) and PE-HD2 (right) for **a** non-exposed and **b** after an UV-radiative exposure $H = 500 \text{ MJ m}^{-2}$ and *P. aeruginosa* after attachment time of 5 min for **c** non-exposed and **d** after UV-radiative exposure $H = 217 \text{ MJ m}^{-2}$.

surfaces and this background fluorescence is more evident on PE-HD2 than on PE-HD1.

Furthermore, *P. aeruginosa* colonizes both non-exposed surfaces more efficiently than *B. subtilis*, although the attachment time for *P. aeruginosa* is reduced by half to $t = 5$ min (Fig. 4c). *P. aeruginosa* also adheres to the UV-exposed surface of PE-HD1 ($H = 217 \text{ MJ m}^{-2}$), but the adhesion of the bacterium on PE-HD2 cannot be visualized and the fluorescence image appears bright white (Fig. 4c, d).

Interestingly, for *B. subtilis*, individual cells could be identified in PE-HD2 ($H = 500 \text{ MJ m}^{-2}$). It is possible that the larger *B. subtilis* cells have a better penetration capacity for DAPI or a higher DNA-content (different numbers of chromosomal/extrachromosomal DNA), leading to a better visualization via fluorescence microscopy⁴⁵.

The UV-irradiation of PE-HD2 leads to a stronger chemical formation of unsaturated carbonyl groups, as demonstrated by the faster carbonyl evolution CI (Fig. 3a). The luminescent species in polyethylene are mainly recognized as α -, β -unsaturated carbonyl groups of the enone type^{4,46,47}. They cause an intrinsic luminescence and overlap with the signal of DAPI-stained cells, resulting in being less visible under a fluorescence microscope.

This is particularly noticeable on strongly photo-oxidized surfaces; due to the higher concentration of unsaturated carbonyl groups this is more apparent on PE-HD2. The progressive intensity of luminescence on the UV-exposed polymers for distinct H is compared in Fig. 5. Both non-exposed PE-HD surfaces exhibit a weak, barely perceptible luminescence emission intensity. This result coincides with the visualization of the fluorescent DAPI stained bacteria on both non-exposed polymer surfaces (Fig. 4a, c).

Both photo-oxidized polymers luminesce; at higher UV-radiative exposures the intrinsic luminescence increases. For the lower UV-exposure of 217 MJ m^{-2} , PE-HD1 showed minimal luminescence ($I_{max} \approx 1$), while the other polyethylene covers a wide emission range λ from 410–700 nm. The maximum intensity is $I_{max} \approx 11.5$. Further UV-exposure of $H = 500 \text{ MJ m}^{-2}$ induced a broad increase in luminescence emission for PE-HD1, but the maximum intensity was three magnitudes lower compared to PE-HD2 ($I_{max} \approx 26$).

The luminescence emission shows on both polymers an intensity maximum centered in the wavelength region λ_{em} from 460–480 nm that increases as photo-oxidation progresses. This is consistent with another study that attributed the emission of unsaturated ketones formed as oxidation to the emission of

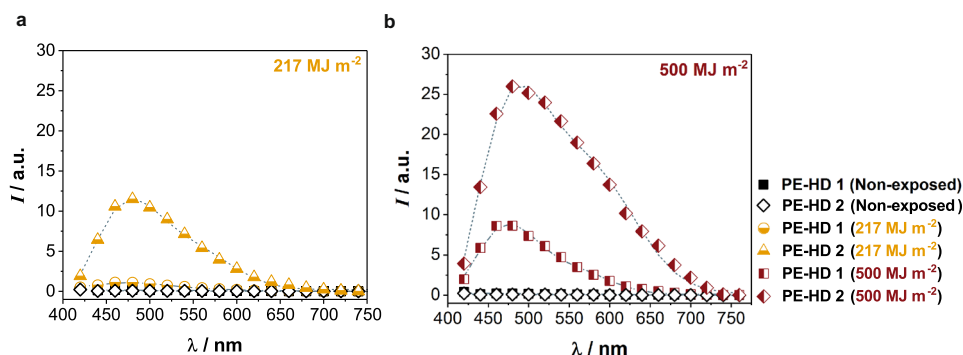


Fig. 5 Luminescence emission intensity. The luminescence emission intensity I for emission wavelength λ in the range 420–780 nm at the excitation wavelength $\Lambda = 405$ nm for both non-exposed PE-HD1 and PE-HD2, compared to **a** UV-radiative exposure H of 217 MJ m^{-2} and **b** 500 MJ m^{-2} .

unsaturated ketones⁹. However, this emission maximum is exactly located in the emission region of the fluorescent dye DAPI ($\lambda_{em} = 461$ nm), causing that the bacteria can no longer be visualized under the fluorescence microscope as surface deterioration of PE-HD progresses.

Changing the staining-dye to wavelength emission regions of green (λ_{em} 560–490 nm) and red (λ_{em} 700–630 nm) is also not possible, since this is also located in the broad emission tail of the photo-oxidized polymers.

Based on the presented results, an evaluation of the initial attachment of bacteria to photo-oxidized polymer surfaces using fluorescence microscopy is only possible to a limited extent. To evaluate both bacteria, *B. subtilis*, and *P. aeruginosa*, regarding their initial adhesion to both UV-damaged polymers, an alternative evaluation method was applied.

Determination of the initial attachment of bacteria by colony forming units (CFU)

Another indirect option for determining adhered cells is the use of CFU. A CFU is derived from a single viable bacterial cell. This cell proliferates and forms a visible colony on an agar plate. This makes it possible to determine the cell number of viable individual cells that were attached to the polymer.

In microbiology, the optical density at a wavelength of 600 nm (OD_{600}) is used to estimate the number of cells in a bacterial suspension. The OD_{600} and the corresponding cell number varies depending on the species-typical cell size and shape. Therefore, the cell number needs to be determined for each individual species.

By using a Neubauer counting chamber it was determined that a cell suspension with an OD_{600} of 0.1 corresponds to 1.61×10^8 cells/ml for *P. aeruginosa* and 9.05×10^6 cells/mL for *B. subtilis*. To obtain comparable results for *B. subtilis* and *P. aeruginosa*, the percentage of adhered cells to the different polymers were calculated. In general, the percentage of adhered *P. aeruginosa* cells was significant higher for all tested polymers independently of UV-treatment, compared to *B. subtilis* (Fig. 4).

Harimawan et al.⁴⁸ conducted similar experiments with *P. aeruginosa* and *B. subtilis*, investigating their attachment affinity to steel in TGY-medium (Tryptone-Glucose-Yeast-Broth). In their experiments, they determined the cell surface charge (ζ -potential) for both bacteria and found that those of *B. subtilis* (-18.1 ± 0.7 mV) was slightly more negative than those of *P. aeruginosa* (-12.4 ± 0.8 mV)⁴⁸. The steel itself had a ζ -potentials of -337 ± 4 mV. TGY-medium is like TSB (Tryptic-Soy-Broth), a rich medium containing glucose as the main carbon and energy source. Since the medium composition of TGY and TSB is comparable, it is likely that *B. subtilis* and *P. aeruginosa* had similar ζ -potentials in our experiments. Comparable to our study, Harimawan et al.⁴⁸

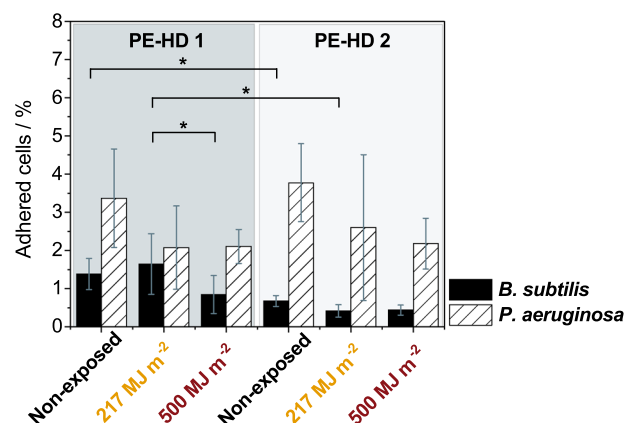


Fig. 6 Detection of the differences of the colonization of UV-exposed polymer by colony forming units. Adhered cells in percentage as determined by CFU for PE-HD1 and PE-HD2 exposed to different UV-radiative exposures H . Black bars represent *B. subtilis*, shaded bars represent *P. aeruginosa* cells, respectively, adhered to either non-exposed PE-HD1 (gray background) or non-exposed PE-HD2 (white background) or PE-HD1 and PE-HD2 that were previously exposed to different UV-radiative exposures H of 217 MJ m^{-2} and 500 MJ m^{-2} , respectively. Standard error of the mean of nine replicates. Significant differences in adherence of bacterial cells are indicated with a star; $p = 0.05$.

observed a better initial adhesion of *P. aeruginosa* than for *B. subtilis*. They concluded that the better adhesion by *P. aeruginosa* can be explained by the lower surface charge. However, it is unlikely that the rather small difference of -5.7 mV (ζ -potential) between *P. aeruginosa* and *B. subtilis* on a surface with a charge of -337 ± 4 mV will have such a large effect⁴⁸. It is more likely that *P. aeruginosa* generally has a better attachment ability than *B. subtilis* e.g. due to differences of the cell surface appendages (pili or flagella) or other adhesion molecules. This would also explain the higher surface coverage for *P. aeruginosa* observed under the fluorescence microscope, even though the incubation time for *B. subtilis* was twice as long as for *P. aeruginosa* (Fig. 4).

Another interesting observation was that *B. subtilis* had a significantly demonstrable preference to attach to PE-HD1 rather than to PE-HD2 (Fig. 6). For reasons of confidentiality, we had no precise material specifications. However, we know that PE-HD1 is better stabilized, e.g., by the high oxidation induction time (OIT, Table 2) and therefore less susceptible to oxidative attacks than PE-HD2^{16,20}. This can also be confirmed by the different course of the carbonyl index CI of both polymers (Fig. 3a). In general, polymer stabilizers, e.g. hindered amine light stabilizers, are added

to prevent the formation of free radicals⁴⁹. Due to the lower concentration of stabilizers, PE-HD2 could have accumulated some oxidation products formed by thermo-oxidation during the manufacturing process at higher temperatures. It is therefore conceivable that there were already a few superoxide and hydroxyl groups on the surface, which were below the detection limit of FT-IR/ATR. *B. subtilis* with a size of $1\ \mu\text{m} \times 2\text{--}3\ \mu\text{m}$ could have been influenced more than *P. aeruginosa* ($0.5\ \mu\text{m} \times 0.7\text{--}1.2\ \mu\text{m}$; data not shown) due to its higher surface area. Alternatively, but less likely the stabilizers themselves might have had an attractive effect on *B. subtilis*. Both reasons could explain the lower number of adherent *B. subtilis* cells on non-exposed PE-HD2.

The affinity of *P. aeruginosa* to PE-HD1 and PE-HD2 was similar, however, the adherence of cells to both polymers tendentially decreased with increasing UV-exposure (Fig. 6). A similar tendency was also present for *B. subtilis*, albeit not as pronounced as for *P. aeruginosa*. For example, $1.38 \pm 0.4\%$ of *B. subtilis* cells adhered to non-exposed PE-HD1 while only $0.85 \pm 0.50\%$ of cells were observed on UV-irradiated PE-HD1 with $500\ \text{MJ m}^{-2}$. The trend for PE-HD2 was similar: $0.68 \pm 0.14\%$ *B. subtilis* cells adhered to the non-exposed polymer and the number decreased to $0.44 \pm 0.13\%$ for the polymer that was UV-exposed with $H = 500\ \text{MJ m}^{-2}$.

UV-irradiation of the polymers leads to an increase of oxidation products on the surface as indicated by the carbonyl index *CI* and the hydroxyl index *HI* (including hydroperoxide among others) (Fig. 3a). Studies that are dealing with the attachment of proteins and cells to modified surfaces showed that both, proteins and bacterial cells, reduce their attachment once the substrate had exposed OH-groups on the surfaces^{50,51}. This effect was observed for both, Gram-positive and Gram-negative bacteria including *P. aeruginosa* and *B. subtilis* and is also confirmed in our study.

In conclusion, in this study two different grades of high-density polyethylene commonly used for polymeric fuel storage tanks were investigated and thereby exposed to various environmental factors that are likely to occur during service lifetime. Our scenario mimics (1) a tank filling with diesel and BD as by immersion experiments, (2) solar exposure of UV radiation in presence of oxygen by photo-oxidative degradation, (3) the potential for microbial contamination by first investigating only the initial adhesion on the different non-exposed PE-HD and (4) on the photo-oxidized PE-HDs.

The results of the immersion experiments revealed a faster and higher fuel uptake for the polymer with a lower crystallinity, here PE-HD1. As to the UV-irradiation on PE-HD, the deteriorated amorphous regions, affected by chemi-crystallization and cross-linking, and the photo-oxidized surface layer on the outer region of the specimens (DLO) clearly reveal a hindrance of fuel mass uptake.

That is indicated by significantly reduced fuel diffusivities and observed changes of maximum obtained fuel saturation concentrations. The photo-oxidized surfaces not only lead to reduced fuel sorption, they also exhibited an extended intrinsic luminescence so that the staining with a fluorescent dye was not appropriate to evaluate the bacterial adhesion on the polymer surface. But analysis based on CFU showed that both, *B. subtilis* and *P. aeruginosa*, may not favor attachment on photo-oxidized PE-HD surfaces. This may be attributed to the increased number of carbonyl groups and possibly also superoxide and hydroxyl groups, which may lead to mutual repulsion of the cells and the photo-oxidized PE-HD. As can be seen from the results of the initial attachment and the subsequent fluorescence microscopy, *P. aeruginosa* could attach better to both polymers than *B. subtilis* although the incubation time for *P. aeruginosa* was only half as long. From this, we conclude that *P. aeruginosa* per se has a better attachment ability. Under the tested conditions, *B. subtilis* showed a preference for binding to PE-HD1, which could be attributed by the higher stabilizer content expected in this material. This could

be either because the stabilizer of PE-HD1 being more attractive for *B. subtilis*, or to PE-HD2 showing already early signs of oxidation damage after the thermal treatment during specimen manufacturing.

METHODS

Materials and fuels

The two commercial PE-HD grades under investigation are applicable as container material including for transport of dangerous goods. Both polymers were supplied by LyondellBasell, Frankfurt/M., Germany, as granules and designated in this study as PE-HD1 and PE-HD2^{16,20}. PE-HD1 possesses an OIT that is longer by a factor of six (OIT at $180\ ^\circ\text{C}$ of 436 min), reflecting a distinctly higher stabilization by antioxidants compared to PE-HD2. The higher crystallinity of PE-HD2, as determined by DSC, is expressed in a slightly lower Charpy impact strength, as well as yield strain and higher yield stress in tensile tests. The characteristic properties of both polymers are compiled in Table 2.

Sheets with thicknesses *h* of 4 and 1 mm were manufactured by compression molding according to the standard procedure of ISO 293⁵² and as described in previous studies^{16,18,20}. The compression molding was performed at a temperature of $180\ ^\circ\text{C}$ and a pressure of 10 MPa for 5 min. The sheets were slowly cooled to room temperature ($15\ \text{K min}^{-1}$) and subsequently annealed at $100\ ^\circ\text{C}$ for 3 h. Specimens were machined from these sheets with dimensions: thickness *h* of 4 mm, width *b* of 10 mm and length *l* of 80 mm for the UV-exposure. Square plate specimens for the initial bacterial adhesion (thickness of 4 mm and length of 10 mm) and round disks of 62 mm diameter and 1 mm thickness for the sorption experiments were punched from neat and pre-UV-exposed plates.

The BD fuel was a pure rapeseed methyl ester without additives and stabilizers. The BD was purchased from ASG Analytik-Service Gesellschaft (Neusäss, Germany). The ester content was >99% (m/m) determined by the supplier according to DIN EN 14103:2011⁵³. The conventional petroleum diesel fuel (D) complying with the specifications of EN 590⁵⁴ was obtained from a local gas station.

Ageing induced by UV-irradiation

UV-irradiation-induced ageing was investigated on sheets (thickness $h = 1\ \text{mm}$) and bulk specimens ($h = 4\ \text{mm}$). The weathering device, Global UV Test 200, from Weiss-Umwelttechnik (Reiskirchen, Germany) was equipped with UV-A 340 nm fluorescent lamps of type 1A according to ISO 4892-3, which show a continuous spectrum with spectral contributions starting at 290 nm through a maximum near 340 nm a tailing in the lower VIS region⁵⁵. The selected fluorescent lamps are mounted in parallel and vertically in the door of the device. The lamps correlate well with the actinic portion of the spectral distribution of solar radiation and only provide little visible or IR contribution so that the radiation heating of the samples above the chamber temperature can be neglected. Inside the weathering device a dry air atmosphere (of below 15% RH) and a constant temperature of $60\ ^\circ\text{C}$ was present. The combination of elevated temperature and UV are synergistic leading to a more severe damage.

The UV-irradiance in the weathering device was about $33\ \text{W m}^{-2}$, which is about one third below the noon irradiance maximum in Central Europe. The highest artificial UV-radiative exposure (the time integral of UV-irradiance) of $H = 500\ \text{MJ m}^{-2}$ was achieved in less than 6 months in the artificial weathering device. This highest artificial UV-exposure corresponds to ~2 years of outdoor exposure in the south of Florida (annual solar radiant exposure of $280\ \text{MJ m}^{-2}$ not considering the higher temperature in the artificial weathering device compared to diurnally and seasonally averaged Florida outdoor temperatures⁵⁶).

All specimens were positioned upright on stainless steel racks. The UV-exposition was conducted one-directional and the UV lamp-facing side of the sample was exposed to much stronger radiation than the backside. Further information regarding artificial weathering can be found in reference¹⁶.

The UV-radiative exposure *H* in MJ m^{-2} was calculated according to Eq. 1.

$$H = \frac{33\ \text{W m}^{-2} \times \text{hours}(h) \times 3600\ (\text{s})}{1,000,000} \quad (1)$$

The UV-radiative exposure *H* for the bulk specimens ($h = 4\ \text{mm}$) were as follows: 38, 74, 110, 145, 217, 278, 357, and $500\ \text{MJ m}^{-2}$, respectively. Initial attachment of bacteria was conducted on non-exposed bulk specimens

and exposed to UV-radiative exposure H of 217 and 500 MJ m⁻². The UV-radiative exposure H for the sheets ($h = 1$ mm) were as follows: 110, 217, 330, and 460 MJ m⁻².

Fuel sorption

Disks with diameter of 62 mm were punched before and after UV-exposure from sheets having a thickness of about $h = 1$ mm. This geometry was chosen in order to approximate the so-called plane-sheet boundary conditions being the prerequisite for the applicability of Eq. 3 as a simplified description of mass-uptake controlled by Fickian diffusion⁵⁷. With another hole of about 10 mm in the center, the discs were stacked up on a glass holder with small glass spacers between them. The holder was then placed into a glass jar (100 mm inner diameter, 200 mm high) filled with BD or diesel (D). The jars were kept at a constant immersion temperature T of 60 °C using a water bath. The mass uptake of the specimens was measured gravimetrically using a weight balance MC 410S Sartorius (Göttingen, Germany). Specimens were weighed immediately after removal from the glass jar and the residual fuel was carefully wiped off with a paper tissue. The fuel concentration c in polyethylene was calculated from the initial specimen mass m_0 and mass m_t at the specific immersion time t (Eq. 2):

$$c = \frac{m_t - m_0}{m_0} \quad (2)$$

Diffusion coefficients D were estimated for the disks ($h = 1$ mm) using Eq. 3 under assumption of a plane sheet geometry^{18,57}.

$$\frac{M_t}{M_\infty} = 1 - 8 \sum_{i=0}^{\infty} \frac{1}{\pi^2 (2i+1)^2} \exp\left\{-\frac{D(2i+1)^2 \pi^2 t}{h^2}\right\} \quad (3)$$

Here, the time-dependent mass uptake of a specimen with thickness l is represented with M_t at a time t and M_∞ being the equilibrium mass uptake. Diffusion coefficients D were determined by fitting the first five terms of the series of Eq. 3 (non-linear curve fitting) with the commercial software Origin 9 (OriginLab, Northampton MA, USA). It should be noted that Eq. 3 is only valid for homogeneous media and Fickian diffusion. Although Fickian behavior was more or less confirmed (Supplementary Fig. 1) the application to the UV-irradiated samples should be considered an approximation. The fuel immersion experiments on disks for non-exposed (0 MJ m⁻²) polymer were conducted in triplicate for PE-HD1 and in duplicate for PE-HD2. Fuel immersion experiments on photo-oxidized polyethylene, e.g. 110, 217, 330, and 460 MJ m⁻², were performed on one disk each. The normalized fuel equilibrium concentrations c_∞^* are indicated with an asterisk * and were calculated taking into account the initial fuel equilibrium concentration for the respective non-exposed polymer saturated in BD and/or diesel.

Carbonyl and hydroxyl index

The evolution of carbonyl and hydroxyl groups on PE-HD after UV-irradiation was followed by Fourier-transform infrared spectroscopy in attenuated total reflection mode (FT-IR/ATR). IR spectra were recorded using the OMNIC software (Version 9) and FT-IR spectrometer Nicolet 6700 (Thermo Scientific) equipped with a diamond ATR crystal and a DTGS KBr detector. The wavenumber range was from 4000 to 400 cm⁻¹, the resolution was 4 cm⁻¹ and the obtained spectra were averaged over 32 scans. Spectra were corrected using the standard ATR correction by a tool provided from the OMNIC software.

The rate of polymer oxidation was monitored by the evolution of the carbonyl and hydroxyl products. The carbonyl index CI was determined as the ratio of the integrated carbonyl band region between 1816 and 1600 cm⁻¹ and the integrated reference absorption band between 2977 and 2865 cm⁻¹^{16,58}. The integrated wavenumber region for the hydroxyl index HI was from 3585 to 3100 cm⁻¹ (related to the same reference). FT-IR/ATR spectra were collected on three different positions on the UV-exposed surface on two bulk specimens each. From the calculated CI and HI an arithmetic mean and a coefficient of variation was determined. The internal reference band having its maximum located at 2912 cm⁻¹ was chosen as it is known to be not influenced by the formation of oxygen containing groups in the polymer matrix⁵⁸.

Density measurements

The Archimedes' principle was used to determine the bulk densities of PE-HD. The analytical balance MC 410S Sartorius (Göttingen, Germany)

was equipped with a density determination kit and liquid n-heptane ($\rho_{n\text{-heptane}} = 0.684$ g cm⁻³). Samples were weighed in air ($m_{\text{air}}, \rho_{\text{air}} = 0.0012$ g cm⁻³) and subsequently in n-heptane ($m_{n\text{-heptane}}$). The densities of PE-HD were calculated according to Eq. 4.

$$\rho = \frac{m_{\text{air}}}{m_{\text{air}} - m_{n\text{-heptane}}} (\rho_{n\text{-heptane}} - \rho_{\text{air}}) + \rho_{\text{air}} \quad (4)$$

The densities were determined using disks with a diameter of 10 mm and a thickness h of about 1 mm, which were punched out of the PE-HD sheets. The determination of density values was performed for non-exposed samples and after UV-radiative exposure H of 110, 217, 330, and 460 MJ m⁻², respectively. The number of investigated samples was $n = 4$, respectively.

Luminescence emission studies

Photo-luminescence emission studies on the PE-HD surfaces were performed using the confocal microscope Leica TCS SP8X (Mannheim, Germany) and the software Leica Application Suite X. The excitation wavelength of the diode laser was $\lambda = 405$ nm. The detected emission wavelength λ ranged from 420 to 760 nm in steps of 20 nm width, respectively. Specimens of 4 mm thickness of both polyethylenes were examined for non-exposed samples and after UV-radiative exposure H of 217 and 500 MJ m⁻², respectively.

Strains and media

P. aeruginosa and *B. subtilis* were cultivated in Tryptic Soy Broth (TSB) Medium (Merck KGaA, Darmstadt) at 30 °C and 120 rpm. Growth of the cells was monitored by measuring the optical density at a wavelength of $\lambda = 600$ nm (OD₆₀₀). Initial adhesion experiments were performed in 50% TSB-Medium and an OD₆₀₀ of 0.1.

Initial attachment

Prior to colonization, the polymers were cleaned with acetone in an ultrasonic bath and sterilized with 70 vol-% ethanol for 30 min. To prevent buoyancy of the polymer during the adhesion-experiment, the polymers were fixated to the bottom of a 24-well plate. For initial adhesion, 2 mL cell suspension of either *P. aeruginosa* or *B. subtilis* with an OD₆₀₀ of 0.1 was added to the polymer and the cells were allowed to colonize for 5 or 10 min, respectively. Non-adhered cells were removed by washing the polymer twice in a phosphate-buffered salt solution (PBS).

Fluorescence microscopy

Analysis of initially adhered bacteria on photo-oxidized PE-HD surfaces were performed on the fluorescence microscope AXIO Imager.M2m from Zeiss (Jena, Germany) equipped with a camera AxioCam 503. The reflector used was 49 DAPI, contrast method fluorescence and 63x magnification and oil ImmersolTM 518F Zeiss.

For the fluorescence microscopic evaluations, the samples were prepared as follows: Adhered bacteria were washed twice with a PBS prepared according to standard recipe from ref. 59. Bacteria were killed using a 5 vol% formaldehyde buffer solution at a temperature of 4 °C for at least 2 h. Bacteria were stained for 30 min using Fluoroshield™ with DAPI (4',6-Diamidino-2-Phenylindole, F6057 from Sigma-Aldrich), autoclaved Milli-Q water and subsequent Roti-Mount FlourCare DAPI to prevent rapid bleaching. The stained bacteria on the polymer surface were covered with a glass slide for analysis by fluorescence microscopy.

Colony forming units

For analysis of initial adhered bacteria on photo-oxidized PE-HD surfaces via CFU, the polymer was placed in a 5 mL reaction tube containing 2 mL PBS and 0.02% Tween® 80. The adhered cells were removed from the polymer surface by sonication for 2.5 min without destroying them. Immediately after sonication, the polymer was removed from the PBS and dilutions of the cell-PBS suspension were plated on Tryptic Soy Agar. After incubation, the colonies were counted, and the number of cells adhered to the polymers was calculated. To obtain comparable results for *P. aeruginosa* and *B. subtilis*, the cell number per milliliter for both bacteria were determined in a suspension with an OD₆₀₀ of 0.1 using a Neubauer counting chamber and the percentage of adhered cells were calculated.

Atomic force microscopy

Samples of PE-HD1 and PE-HD2, non-exposed and after an UV-radiative exposure H of 217 MJ m^{-2} and 500 MJ m^{-2} , respectively, were cleaned with acetone and ethanol in an ultrasonic bath. An atomic force microscope NanoWizard 4 (JPK Bruker, Germany) was used to measure height profiles. Sections of $(50 \times 50) \mu\text{m}^2$ were scanned in air with contact mode using the fast scanning mode. Cantilever ContGB-G (Budgetsensors, Bulgaria) with a spring constant of 0.2 N m^{-1} and a resonance frequency of 13 kHz were used. Calibration of the cantilever was performed with the contact-free method according to ref. ⁶⁰. The setpoint was 25 nN and the line rate 2 Hz . Three different areas were measured on each sample and the determination of the root mean square roughness R_q was performed with the JPK Processing software based on the height profiles.

UV-vis spectroscopy

Absorption spectroscopy in the wavelength range between 220 and 850 nm were carried out using a Cary 300 double monochromator spectrometer from Varian/Agilent company (Mulgrave, Australia) in transmission geometry using double channel measurements. The detection limit is about six absorption units. As the PE-HD samples of a thickness h of 4 mm exhibit considerable straylight an integrating sphere of 70 mm diameter with Spectralon coating of the type DRA-CA-30I from Labsphere company (Noth Sutton, USA) was applied in the sample compartment with the sample mounted on the transmission port, in front of a mask of 13 mm height and 0.5 mm width. The integrating sphere conducts all radiation that has passed through the sample to the detector regardless of the incident angle. However, reflection and straylight caused in front of the sample and straylight within the sample still reduce the measured radiation in the sphere. This situation though represents the conditions of a good within a tank and this also is the reason why the measured entity is labeled absorbance rather than absorption. Spectral bandwidth was 4 nm , data interval was 1 nm . The switch-over point between the UV-range deuterium lamp and the visible-range halogen lamp was at 350 nm . A baseline correction for 100% transmission was used for the spectra. The monochromator's scan speed was signal/noise ratio controlled and resulted in an acquisition time of about $60\text{--}120 \text{ min}$ per spectrum.

DATA AVAILABILITY

The data that support the findings of this study are available from the corresponding author upon reasonable request.

Received: 18 December 2019; Accepted: 2 June 2020;
Published online: 09 July 2020

REFERENCES

- Vert, M. et al. Terminology for biorelated polymers and applications (IUPAC Recommendations 2012). *Pure Appl. Chem.* **84**, 377–410 (2012).
- Bolland, J. L. & Gee, G. Kinetic studies in the chemistry of rubber and related materials. II. The kinetics of oxidation of unconjugated olefins. *Trans. Faraday Soc.* **42**, 236–243 (1946).
- Gijsman, P., Meijers, G. & Vitarelli, G. Comparison of the UV-degradation chemistry of polypropylene, polyethylene, polyamide 6 and polybutylene terephthalate. *Polym. Degrad. Stab.* **65**, 433–441 (1999).
- Rabek, J. F. *Photodegradation of polymers: physical characteristics and applications* (Springer, 1996).
- Allen, N. S. et al. Ageing and spectroscopic properties of polyethylenes: comparison with metallocene polymer. *Polym. Degrad. Stab.* **67**, 57–67 (2000).
- Charlesby, A. & Partridge, R. H. The identification of luminescence centres in polyethylene and other polymers. *Proc. R. Soc. A.* **283**, 312–328 (1965).
- Amin, M. U., Scott, G. & Tillekeratne, L. M. K. Mechanism of the photo-initiation process in polyethylene. *Eur. Polym. J.* **11**, 85–89 (1975).
- Gardette, M. et al. Photo- and thermal-oxidation of polyethylene: comparison of mechanisms and influence of unsaturation content. *Polym. Degrad. Stab.* **98**, 2383–2390 (2013).
- Grabmayer, K. et al. Accelerated aging of polyethylene materials at high oxygen pressure characterized by photoluminescence spectroscopy and established aging characterization methods. *Polym. Degrad. Stab.* **109**, 40–49 (2014).
- Grabmayer, K. et al. Characterization of the aging behavior of polyethylene by photoluminescence spectroscopy. *Polym. Degrad. Stab.* **107**, 28–36 (2014).

- Fayolle, B., Richaud, E., Colin, X. & Verdu, J. Review: degradation-induced embrittlement in semi-crystalline polymers having their amorphous phase in rubbery state. *J. Mater. Sci.* **43**, 6999–7012 (2008).
- Craig, I. H., White, J. R., Shyichuk, A. V. & Syrotynska, I. Photo-induced scission and crosslinking in LDPE, LLDPE, and HDPE. *Polym. Eng. Sci.* **45**, 579–587 (2005).
- Fayolle, B., Audouin, L. & Verdu, J. Oxidation induced embrittlement in polypropylene—a tensile testing study. *Polym. Degrad. Stab.* **70**, 333–340 (2000).
- Audouin, L., Langlois, V., Verdu, J. & de Bruijn, J. C. M. Role of oxygen diffusion in polymer ageing: kinetic and mechanical aspects. *J. Mater. Sci.* **29**, 569–583 (1994).
- Mendes, L. C., Rufino, E. S., de Paula, F. O. C. & Torres, A. C. Jr Mechanical, thermal and microstructure evaluation of HDPE after weathering in Rio de Janeiro City. *Polym. Degrad. Stab.* **79**, 371–383 (2003).
- Erdmann, M., Niebergall, U., Wachtendorf, V. & Böhning, M. Evaluation of UV-induced embrittlement of PE-HD by Charpy impact test. *J. Appl. Polym. Sci.* <https://doi.org/10.1002/app.49069> (2020).
- Richaud, E., Flaconnèche, B. & Verdu, J. Biodiesel permeability in polyethylene. *Polym. Test.* **31**, 1070–1076 (2012).
- Böhning, M., Niebergall, U., Adam, A. & Stark, W. Impact of biodiesel sorption on mechanical properties of polyethylene. *Polym. Test.* **34**, 17–24 (2014).
- Böhning, M., Niebergall, U., Zanotto, M. & Wachtendorf, V. Impact of biodiesel sorption on tensile properties of PE-HD for container applications. *Polym. Test.* **50**, 315–324 (2016).
- Erdmann, M., Böhning, M. & Niebergall, U. Physical and chemical effects of biodiesel storage on high-density polyethylene: evidence of co-oxidation. *Polym. Degrad. Stab.* **161**, 139–149 (2019).
- Saad, A. K., Gomes, F. P. C. & Thompson, M. R. Plasticizing effect of oxidized biodiesel on polyethylene observed by nondestructive method. *Fuel* **252**, 246–253 (2019).
- Thompson, M. R. et al. Long term storage of biodiesel/petrol diesel blends in polyethylene fuel tanks. *Fuel* **108**, 771–779 (2013).
- Erdmann, M. et al. Diesel-induced transparency of plastically deformed high-density polyethylene. *J. Mater. Sci.* **54**, 11739–11755 (2019).
- Richaud, E., Fayolle, B., Verdu, J. & Rychlý, J. Co-oxidation kinetic model for the thermal oxidation of polyethylene-unsaturated substrate systems. *Polym. Degrad. Stab.* **98**, 1081–1088 (2013).
- Richaud, E., Djouani, F., Fayolle, B., Verdu, J. & Flaconnèche, B. New Insights in polymer-biofuels interaction. *Oil Gas. Sci. Technol. – Rev. IFP Energ. nouvelles* **70**, 17 (2015).
- Gaylarde, C. C., Bento, F. M. & Kelley, J. Microbial contamination of stored hydrocarbon fuels and its control. *Rev. de Microbiologia.* **30**, 01–10 (1999).
- Passman, F. J. Microbial contamination and its control in fuels and fuel systems since 1980—a review. *Int. Biodeterior. Biodegrad.* **81**, 88–104 (2013).
- Martin-Sanchez, P. M., Gorbushina, A. A. & Toepel, J. Quantification of microbial load in diesel storage tanks using culture- and qPCR-based approaches. *Int. Biodeterior. Biodegrad.* <https://doi.org/10.1016/j.ibiod.2016.04.009> (2016).
- Bento, F. M. & Gaylarde, C. C. Biodeterioration of stored diesel oil: studies in Brazil. *Int. Biodeterior. Biodegrad.* **47**, 107–112 (2001).
- Restrepo-Florez, J. M., Bassi, A., Rehmann, L. & Thompson, M. R. Investigation of biofilm formation on polyethylene in a diesel/biodiesel fuel storage environment. *Fuel* **128**, 240–247 (2014).
- Restrepo-Florez, J. M., Bassi, A. & Thompson, M. R. Microbial degradation and deterioration of polyethylene—a review. *Int. Biodeterior. Biodegrad.* **88**, 83–90 (2014).
- Fregolente, P. B. L., Fregolente, L. V. & Wolf Maciel, M. R. Water content in biodiesel, diesel, and biodiesel–diesel blends. *J. Chem. Eng. Data.* **57**, 1817–1821 (2012).
- Oliveira, M. B., Varanda, F. R., Marrucho, I. M., Queimada, A. J. & Coutinho, J. A. P. Prediction of water solubility in biodiesel with the CPA equation of state. *Ind. Eng. Chem. Res.* **47**, 4278–4285 (2008).
- Martin-Sanchez, P. M., Becker, R., Gorbushina, A. A. & Toepel, J. An improved test for the evaluation of hydrocarbon degradation capacities of diesel-contaminating microorganisms. *Int. Biodeterior. Biodegrad.* **129**, 89–94 (2018).
- Abrusci, C. et al. Biodegradation of photo-degraded mulching films based on polyethylenes and stearates of calcium and iron as pro-oxidant additives. *Int. Biodeterior. Biodegrad.* **65**, 451–459 (2011).
- Arkatkar, A., Juwarkar, A. A., Bhaduri, S., Uppara, P. V. & Doble, M. Growth of *Pseudomonas* and *Bacillus* biofilms on pretreated polypropylene surface. *Int. Biodeterior. Biodegrad.* **64**, 530–536 (2010).
- Goulter, R. M., Gentle, I. R. & Dykes, G. A. Issues in determining factors influencing bacterial attachment: a review using the attachment of *Escherichia coli* to abiotic surfaces as an example. *Lett. Appl. Microbiol.* **49**, 1–7 (2009).
- Marshall, K. C., Stout, R. & Mitchell, R. Mechanism of the initial events in the sorption of marine bacteria to surfaces. *Microbiology* **68**, 337–348 (1971).

39. Garrett, T. R., Bhakoo, M. & Zhang, Z. Bacterial adhesion and biofilms on surfaces. *Prog. Nat. Sci.* **18**, 1049–1056 (2008).
40. Menrad, A., Goedecke, T., Gruender, K.-P. & Wagner, M. H. The internal pressure test in experiment and simulation—influence of the wall thickness variation and the change of the packaging behavior after the impact of standard liquids. *Packaging Technol. Sci.* **26**, 311–326 (2013).
41. SAE. J2665—Surface vehicle recommended practice: test procedure to measure fuel permeability of materials by the cup weight loss method (SAE, 2006).
42. Gillen, K. T., Celina, M. & Clough, R. L. Density measurements as a condition monitoring approach for following the aging of nuclear power plant cable materials. *Radiat. Phys. Chem.* **56**, 429–447 (1999).
43. Gulmine, J. V., Janissek, P. R., Heise, H. M. & Akcelrud, L. Degradation profile of polyethylene after artificial accelerated weathering. *Polym. Degrad. Stab.* **79**, 385–397 (2003).
44. Kömmling, A., von der Ehe, K., Wolff, D. & Jaunich, M. Effect of high-dose gamma irradiation on (U)HMWPE neutron shielding materials. *Radiat. Phys. Chem.* **142**, 29–33 (2018).
45. Ross, J., Boon, P. I., Sharma, R. & Beckett, R. Variations in the fluorescence intensity of intact DAPI-stained bacteria and their implications for rapid bacterial quantification. *Lett. Appl. Microbiol.* **22**, 283–287 (1996).
46. Allen, N. S. Light absorbing species in polyolefins: a fluorescence/derivative UV spectroscopy study. *Polym. Degrad. Stab.* **6**, 193–200 (1984).
47. Allen, N. S., Homer, J., McKellar, J. F. & Wood, D. G. M. Identification of the luminescent species in low-density polyethylene. *J. Appl. Polym. Sci.* **21**, 3147–3152 (1977).
48. Harimawan, A., Rajasekar, A. & Ting, Y.-P. Bacteria attachment to surfaces—AFM force spectroscopy and physicochemical analyses. *J. Colloid Interface Sci.* **364**, 213–218 (2011).
49. Chirinos Padron, A. J. Performance and mechanisms of hindered amine light stabilizers in polymer photostabilization. *J. Macromol. Sci. Part C.* **30**, 107–154 (1990).
50. Weinhart, M. et al. Linear and hyperbranched polyglycerol derivatives as excellent bioinert glass coating materials. *Adv. Eng. Mater.* **13**, B501–B510 (2011).
51. Guo, J.-S. et al. Microbial attachment and adsorption–desorption kinetic of tightly bound extracellular polymeric substances on model organic surfaces. *Chem. Eng. J.* **279**, 516–521 (2015).
52. ISO 293:2004 Plastics—compression moulding of test specimens of thermoplastic materials (2004).
53. DIN EN 14103:2011-07 Fat and oil derivatives - Fatty Acid Methyl Esters (FAME) - Determination of ester and linolenic acid methyl ester contents; German version EN 14103:2011 (2011).
54. DIN EN 590:2014-04 - Automotive fuels - Diesel - Requirements and test methods; German version EN 590:2013 + AC:2014. (2014).
55. ISO 4892-3:2013 Plastics - methods of exposure to laboratory light sources - Part 3: Fluorescent UV lamps (2013).
56. Atlas. <https://www.atlas-mts.com/products/testingservices/natural-weathering/natural-weathering-testing-sites/north-american-sites/florida-benchmark-testing-sites> (2018).
57. Crank, J. *The Mathematics of Diffusion*. 2nd ed. Vol. 10 (Oxford University Press, 1975).
58. Stark, N. M. & Matuana, L. M. Surface chemistry changes of weathered HDPE/wood-flour composites studied by XPS and FTIR spectroscopy. *Polym. Degrad. Stab.* **86**, 1–9 (2004).
59. Sambrook, J. & Russell, D. W. *Molecular Cloning: A Laboratory Manual*. 3rd ed. Vol. 3 (Cold Spring Harbor Laboratory Press, 2001).
60. Sader, J. E. et al. Spring constant calibration of atomic force microscope cantilevers of arbitrary shape. *Rev. Sci. Instrum.* **83**, 103705 (2012).

ACKNOWLEDGEMENTS

This research was financed by the BAM-internal project “Microbial influenced Corrosion” (MIC) in the focus area “Material” with special thanks to Jörg Toepel. The authors further would like to thank Oliver Schwarze, Nicolai Schmidt and Michael Schneider for sample preparation. We kindly acknowledge Janin Sameith and Anna Sommer for their assistance in fluorescence microscopic experiments and Biwen Annie An for data discussion.

AUTHOR CONTRIBUTIONS

U.N., M.B. and A.K. supervised the study. M.E. and V.W. performed the UV-exposure of the polymers. M.E. conducted the FT-IR/ATR measurements and V.W. and M.B. contributed to the discussion of the data. M.E. performed the fuel uptake measurements and M.B., V.W., and U.N. contributed to the data discussion. S.K., M.E., and A.K. contributed to the preparation of the initial bacterial adhesion experiments. M.E. and A. K. supervised the fluorescence microscopy. M.E. and A.K. conducted and analyzed the luminescence measurements, V.W. contributed to the data analysis. S.K. conducted the initial bacterial adhesion experiments and A.K. contributed to the data analysis. J.D.S. conducted the AFM measurements. V.W. performed the UV-vis spectroscopy. V.W. and M.E. contributed to the data analysis. M.E., A.K., and S.K. wrote the manuscript with contributions of all other authors. All authors contributed to the editing of the paper, and approval of the content in its current form.

COMPETING INTERESTS

The authors declare no competing interests.

ADDITIONAL INFORMATION

Supplementary information is available for this paper at <https://doi.org/10.1038/s41529-020-0122-1>.

Correspondence and requests for materials should be addressed to A.K.

Reprints and permission information is available at <http://www.nature.com/reprints>

Publisher's note Springer Nature remains neutral with regard to jurisdictional claims in published maps and institutional affiliations.



Open Access This article is licensed under a Creative Commons Attribution 4.0 International License, which permits use, sharing, adaptation, distribution and reproduction in any medium or format, as long as you give appropriate credit to the original author(s) and the source, provide a link to the Creative Commons license, and indicate if changes were made. The images or other third party material in this article are included in the article's Creative Commons license, unless indicated otherwise in a credit line to the material. If material is not included in the article's Creative Commons license and your intended use is not permitted by statutory regulation or exceeds the permitted use, you will need to obtain permission directly from the copyright holder. To view a copy of this license, visit <http://creativecommons.org/licenses/by/4.0/>.

© The Author(s) 2020